Mohammad Sefid
Associate Professor
School of Mechanical Engineering,
Yazd University,
Yazd 89195-741, Iran
e-mail: mhsefid@yazd.ac.ir

Rouhollah Fatehi
Assistant Professor
Department of Mechanical Engineering,
School of Engineering,
Persian Gulf University,
Bushehr 75169, Iran
e-mail: fatehi@pgu.ac.ir

Rahim Shamsoddini[1]
School of Mechanical Engineering,
Yazd University,
Yazd 89195-741, Iran
e-mail: shamsoddini@stu.yazd.ac.ir

A Modified Smoothed Particle Hydrodynamics Scheme to Model the Stationary and Moving Boundary Problems for Newtonian Fluid Flows

A robust modified weakly compressible smoothed particle hydrodynamics (WCSPH) method based on a predictive corrective scheme is introduced to model the fluid flows engaged with stationary and moving boundary. In this paper, this model is explained and practically verified in three distinct laminar incompressible flow cases; the first case involves the lid driven cavity flow for two Reynolds numbers 400 and 1000. The second case is a flow generated by a moving block in the initially stationary fluid. The third case is flow around the stationary and transversely oscillating circular cylinder confined in a channel. These results in comparison with the standard benchmarks also confirm the good accuracy of the present solution algorithm. [DOI: 10.1115/1.4028643]

1 Introduction

Smoothed particle hydrodynamics (SPH) method was first proposed for astrophysical applications by Lucy [1] and Gingold and Monaghan [2]. It was gradually extended to model a wide range of engineering applications including elasticity [3], multiphase flows [4], and blood simulation [5]. The SPH method has also widely been used to model the incompressible flows using an appropriate equation of state which relates the variations of the pressure to the variations of the density [6,7]. This approach is known as "WCSPH." Another approach entitled "incompressible smoothed particle hydrodynamics (ISPH)" applies a two-step projection method which first calculates the predicted velocity and then corrects the predicted one by the pressure obtained by solving the Poisson equation. The early works, which used the latter method, are done by Cummins and Rudman [8] and Shao and Lo [9]. In this method, the pressure equation is solved in the same way offered by Koshizuka and Oka [10] for moving particle semi-implicit method. Each of the above methods has their own advantages and disadvantages; although the WCSPH is implemented easily, Lee et al. [11] showed that the standard WCSPH has wide pressure fluctuations. They reported that ISPH yields much more reliable results than standard WCSPH; velocity and pressure fields, in particular, are smoother in every case. However, the solution of Poisson pressure equation is a time consuming process. Some corrections were offered to improve both of the methods. Bonet and Lok [12] and Rodriguez-Paz and Bonet [13] proposed and applied corrected SPH methods. One of the most important aspects of their corrections was the improvement of the accuracy of kernel gradient used to discretize the first spatial derivatives. Shadloo et al. [14] showed that WCSPH can handle complex geometries using the multiple boundary tangents method and eliminate particle clustering-induced instabilities with the implementation of a particle fracture repair procedure as well as the corrected SPH discretization scheme. Using a modified renormalization tensor, Fatehi and Manzari [15] proposed a new SPH scheme for approximating second derivatives that has the property of first-order consistency. In other studies, they also proposed a remedy for nonphysical oscillations in WCSPH [16]. For ISPH, Hu and Adams [17,18] proposed a constant-density constraint which has not been achieved by previous projection SPH methods.

Some corrections, which improve accuracy and stability of the SPH method, were mentioned above. Now, it can be stated that WCSPH gives also quite accurate results as much as ISPH by adding the proper numerical treatments to the numerical scheme like density correction algorithms or the addition of density diffusion terms to the mass conversation equation or particle shifting algorithms.

Since SPH has the Lagrangian nature and is based on particles, it is suitable to model the complex phenomena such as free surface [19,20], two phase flow [4], moving boundary and fluid–structure interactions (FSIs) [21–24]. The last one has its own complexity for other numerical methods especially for the Eulerian and grid-based methods; immersed boundary [25,26] and arbitrary Lagrangian Eulerian (ALE) method [27] are the approaches which are used for the grid-based methods. Therefore, some investigations of the moving boundary and FSI problems has been recently done using the SPH method; Kajtar and Monaghan [21] described how the swimming of linked-rigid bodies can be simulated using SPH. To simulate two way coupled FSI, Hashemi et al. [22,23] coupled the immersed boundary method with SPH method for the Newtonian and non-Newtonian fluid. Cohen et al. [24] simulated the dolphin kick swimming by SPH to evaluate variants of this swimming stroke technique.

In the present study, an algorithm is introduced which can be useful for modeling the complex problems such as moving boundary and one way FSI problems. In this algorithm, using the mass conservation equation, the divergence of velocity is related to the Laplacian of pressure. This pressure–velocity coupling causes to remove the nonphysical fluctuations [16]. In addition, the kernel gradient is renormalized using the first-order derivatives corrective tensor. To avoid the tensile instability and defects phenomena, a shifting procedure is considered. Although these were separately examined, a combination of these modifications leads to a robust and consistent WCSPH. To show the capability of the model, it is applied and verified for three distinct laminar and incompressible flow cases engaged with stationary and moving boundaries; the first case involves the flow in a lid driven cavity

[1]Corresponding author.

Contributed by the Fluids Engineering Division of ASME for publication in the Journal of Fluids Engineering. Manuscript received December 24, 2013; final manuscript received September 20, 2014; published online October 21, 2014. Assoc. Editor: Zhongquan Charlie Zheng.

for two Reynolds numbers 400 and 1000. Then the effect of number of particles on the convergence and accuracy is investigated. The second case is the flow induced by a moving block in the initially stationary fluid in a rectangular cavity which is the well-known sixth SPHERIC benchmark [28]. The third case involves the simulation of the flow around a confined circular cylinder in a channel with the periodic boundary condition.

In the following, first the governing equations and numerical algorithm are discussed. Then the results and discussions including three cases for verification of the proposed algorithm are presented.

2 Governing Equations and Numerical Procedure

2.1 Formulation. The formulation of the SPH method is based on an integral form which indicates each continuous defined function over an interest domain Ω can be stated as

$$f(r) = \int_{\Omega} f(r')W(r - r', h)dr' \tag{1}$$

where r and r' are position vector and subintegral variable, respectively, h is the smoothing length, and W is the weight or kernel function. The above equation can be approximated by a numerical summation on the discrete points in the domain Ω

$$f(r) = \sum_j \forall_j f_j W(r - r_j, h) \tag{2}$$

where $\forall_j$ is the volume of jth particle. In the present study, the fifth-order Wendland kernel is used. Recent studies have shown that the use of this Kernel function causes to increase the accuracy [29].

$$W(r,h) = W_0 \times \begin{cases} \left(1 - \frac{|r|}{h}\right)^4 \left(4\frac{|r|}{h} + 1\right) & 0 \le \frac{|r|}{h} < 1 \\ 0 & \frac{|r|}{h} \ge 1 \end{cases} \tag{3}$$

where W_0 is $7/\pi h^2$ for two-dimensional cases.

In the present study, the gradient, divergence, and Laplacian operator for an arbitrary scalar function f or tensor function $\boldsymbol{F}$ are, respectively, calculated as

$$\langle \nabla f \rangle_i = \sum_j \forall_j (f_j - f_i)\boldsymbol{B}_i . \nabla W_{ij} \tag{4}$$

$$\langle \nabla \cdot \boldsymbol{F} \rangle_i = \sum_j \forall_j (\boldsymbol{F}_j - \boldsymbol{F}_i) \cdot (\boldsymbol{B}_i \cdot \nabla W_{ij}) \tag{5}$$

$$\langle \nabla^2 f \rangle_i = \sum_j 2\forall_j \frac{f_i - f_j}{r_{ij}} \boldsymbol{e}_{ij} \cdot (\boldsymbol{B}_i \cdot \nabla W_{ij}) \tag{6}$$

where $\boldsymbol{e}_{ij}$ is the unit vector in the interparticle direction (from j to i) and B is a corrective tensor for kernel gradients which was before applied and examined by Bonet and Lok [12]

$$\boldsymbol{B}_i = -\left[\sum_j \forall_j r_{ij} \nabla W_{ij}\right]^{-1} \tag{7}$$

The governing equations for the fluid flow are, respectively, mass, momentum, and the state equations

$$\frac{d\rho}{dt} = -\rho \nabla \cdot \boldsymbol{V} \tag{8}$$

$$\rho \frac{d\boldsymbol{V}}{dt} = \mu \nabla^2 \boldsymbol{V} + \rho \boldsymbol{g} - \nabla p \tag{9}$$

$$p - p_0 = C^2(\rho - \rho_0) \tag{10}$$

where ρ, V, p, μ, and C are, respectively, the fluid's density, velocity, pressure, viscosity, and speed of sound. Discretizing and solving the above equations according to the SPH formulations lead to the standard WCSPH method. The discretized equations for WCSPH are as follows:

$$\rho_i^{n+1} = \rho_i^n (1 - \Delta t \langle \nabla \cdot \boldsymbol{V}^n \rangle_i) \tag{11}$$

$$(p_i^{n+1} - p_0) = C^2(\rho_i^{n+1} - \rho_0) \tag{12}$$

$$\boldsymbol{V}_i^{n+1} = \boldsymbol{V}_i^n + \left(\boldsymbol{g} + \langle \nu \nabla^2 \boldsymbol{V}^n \rangle_i - \left\langle \frac{\nabla p^{n+1}}{\rho} \right\rangle_i\right) \Delta t \tag{13}$$

$$\boldsymbol{r}_i^{n+1} = \boldsymbol{r}_i^n + \boldsymbol{V}_i^{n+1} \Delta t \tag{14}$$

where $\boldsymbol{r}$ is the particle position vector, n refers to previous time-step, and $n+1$ refers to present time-step.

2.2 Predictive Corrective Scheme. As mentioned before, the standard WCSPH suffers from the pressure and density fluctuations [11]. Fatehi and Manzari [16] showed that the velocity–pressure coupling reduces the nonphysical fluctuations. So a pseudoconstant density algorithm is applied to remove the density and pressure fluctuations to improve the WCSPH. The present method has been based on a predictor–corrector scheme

Predictor Step: The discretization of the conservation of mass (Eq. (8)) leads to

$$\frac{\rho_i^{*,n+1} - \rho_i^n}{\alpha \Delta t} = -\rho_i^n \left\langle \nabla \cdot \boldsymbol{V}^{n+1/2} \right\rangle_i \Rightarrow \frac{\frac{m_i}{\forall_i^{*,n+1}} - \frac{m_i}{\forall_i^n}}{\alpha \Delta t} = -\frac{m_i}{\forall_i^n} \left\langle \nabla \cdot \boldsymbol{V}^{n+1/2} \right\rangle_i \tag{15}$$

m_i is constant, so the conservation of mass leads to

$$\frac{1}{\forall_i^{*,n+1}} = \frac{1}{\forall_i^n} \left(1 - \alpha \Delta t \left\langle \nabla \cdot \boldsymbol{V}^{n+1/2} \right\rangle_i\right) \tag{16}$$

where α is a coefficient which can vary between 0 and 1 and is the ratio between the previous time-step (n) and intermediate time step ($^*, n+1$) and $\boldsymbol{V}^{n+1/2}$ is the intermediate velocity. Dividing Eq. (9) by ρ leads to

$$\frac{d\boldsymbol{V}}{dt} = \nu \nabla^2 \boldsymbol{V} + \boldsymbol{g} - \frac{\nabla p}{\rho} \tag{17}$$

where ν is the kinematic viscosity. The right-hand side terms of Eq. (17) are, respectively, acceleration terms due to viscous, buoyancy and pressure forces. The SPH discretization of the above equation will be

$$\frac{\boldsymbol{V}_i^{n+1} - \boldsymbol{V}_i^n}{\Delta t} = \left(\boldsymbol{g} + \langle \nu \nabla^2 \boldsymbol{V}^n \rangle_i - \left\langle \frac{\nabla p}{\rho} \right\rangle_i^n\right) \tag{18}$$

So, the intermediate velocity can be defined as

$$\boldsymbol{V}_i^{n+1/2} = \boldsymbol{V}_i^{*,n+1} - \alpha \Delta t \left\langle \frac{\nabla p^n}{\rho} \right\rangle_i \tag{19}$$

where $\boldsymbol{V}_i^{*,n+1}$ is the part of intermediate velocity which is caused by the buoyancy and viscous terms of fluid particle acceleration

$$\boldsymbol{V}_i^{*,n+1} = \boldsymbol{V}_i^n + \left(\boldsymbol{g} + \langle \nu \nabla^2 \boldsymbol{V}^n \rangle_i\right) \alpha \Delta t \tag{20}$$

Applying the divergence operator in Eq. (19)

$$\left\langle \nabla \cdot \boldsymbol{V}^{n+1/2} \right\rangle_i = \left\langle \nabla \cdot \boldsymbol{V}^{*,n+1} \right\rangle_i - \alpha \Delta t \left\langle \nabla \cdot \frac{\nabla p^n}{\rho} \right\rangle_i \tag{21}$$

and substituting in Eq. (16) leads to

$$\frac{1}{\forall_i^{*,n+1}} = \frac{1}{\forall_i^n} \left(1 - \alpha \Delta t \left(\left\langle \nabla \cdot \boldsymbol{V}^{*,n+1} \right\rangle_i - \alpha \Delta t \left\langle \nabla \cdot \frac{\nabla p^n}{\rho} \right\rangle_i \right) \right) \tag{22}$$

Then, according to Eqs. (12) and (22), the pressure at the next time-step is calculated by

$$p_i^{n+1} = p_0 + C^2 \left(\frac{m_i}{\forall_i^n} \left(1 - \alpha \Delta t \left(\left\langle \nabla \cdot \boldsymbol{V}^{*,n+1} \right\rangle_i - \alpha \Delta t \left\langle \nabla \cdot \frac{\nabla p^n}{\rho} \right\rangle_i \right) \right) - \rho_0 \right) \tag{23}$$

Corrector Step: The process defined in the predictor step is only carried out to calculate the pressure. The final velocity, volume, and position of each particle for the new time-step are determined in the corrector step; the velocity of each particle is updated using pervious velocity and current pressure gradient

$$\boldsymbol{V}_i^{n+1} = \boldsymbol{V}_i^n + \left(\boldsymbol{g} + \left\langle \nu \nabla^2 \boldsymbol{V}^n \right\rangle_i - \left\langle \frac{\nabla p^{n+1}}{\rho} \right\rangle_i \right) \Delta t \tag{24}$$

Then, the new volume and density are, respectively, calculated by

$$\frac{1}{\forall_i^{n+1}} = \frac{1}{\forall_i^{*,n+1}} \left(1 - (1 - \alpha) \Delta t \left\langle \nabla \cdot \boldsymbol{V}^{n+1/2} \right\rangle_i \right) \tag{25}$$

$$\rho_i^{n+1} = \frac{m_i}{\forall_i^{n+1}} \tag{26}$$

Finally, the particle position is rearranged by

$$\boldsymbol{r}_i^{n+1} = \boldsymbol{r}_i^n + \boldsymbol{V}_i^{n+1} \Delta t \tag{27}$$

Beside from the modified discretization scheme (6), the basic difference between the standard WCSPH and proposed algorithms is in the calculation of the divergence of the velocity for calculating the density; the standard WCSPH uses the divergence of the velocity of the previous time-step, while the proposed algorithm uses the divergence of the intermediate velocity and Laplacian of the previous time-step pressure.

2.3 Calculation Time-Step. The time-step ($\Delta t = t^{n+1} - t^n$) is calculated from the equation

$$\Delta t = \beta_t \min \left(\frac{\delta_{\min}}{U_{\max}}, \frac{\delta_{\min}^2}{\upsilon}, \sqrt{\frac{\delta_{\min}}{g}} \right) \tag{28}$$

where β_t is a constant coefficient which can be between 0 and 1, $\delta_{\min}$ is the minimum distance between two neighboring particles, $U_{\max} = C + V_{\max}$ and $V_{\max}$ is the maximum velocity of the particles. The first term is obtained from the Courant–Friedrichs–Lewy (CFL) condition which states that $U_{\max} \Delta t / \delta_{\min}$ should be less than 1. The second term is imposed for stability of the viscous term and the third one is defined to satisfy the stability of body force acceleration term in the momentum equation. Similar formulation has been proposed by Morris et al. [30]. However, they used smoothing length (h) as the characteristic length scale, while the minimum particle space ($\delta_{\min}$) is considered as the characteristic length scale in the present study. Whereas $\delta_{\min}$ is much less than h, $\delta_{\min}$ can be more proper as the characteristic length scale.

2.4 Shifting Particles. Tensile instability, defects, and particles' clustering are complications in the SPH simulations. To avoid the mentioned phenomena, a shifting algorithm similar to the particle shifting strategy of Xu et al. [31] has been applied in the present study. The direction and amount of shifting are determined from the arrangement of neighboring particles; the $\Delta \boldsymbol{r}_i$ is defined as shifting particle vector which is calculated by

$$\Delta \boldsymbol{r}_i = \varepsilon \bar{\boldsymbol{r}}_i \tag{29}$$

where ε can vary between 0 and 0.1 and $\bar{\boldsymbol{r}}_i$ is equal to

$$\bar{\boldsymbol{r}}_i = \sum_j \forall_j \boldsymbol{r}_{ij} W_{ij} \tag{30}$$

If the particles are homogeneously distributed around the particle i, then $\bar{\boldsymbol{r}}_i$ will be zero. Otherwise this vector shows that the distribution of neighboring particles around the particle is not balanced. Then the particle is slightly shifted by $\Delta \boldsymbol{r}_i$. Ultimately, it is necessary to modify the flow field variables in the new position. These modifications according to the first-order Taylor series expansion are

$$\Delta \boldsymbol{V}_i = \Delta \boldsymbol{r}_i . \langle \nabla \boldsymbol{V} \rangle_i \tag{31}$$

$$\Delta p_i = \rho_i \Delta \boldsymbol{r}_i . \left\langle \frac{\nabla p}{\rho} \right\rangle_i \tag{32}$$

$$\Delta \rho_i = \frac{\Delta p_i}{C^2} \tag{33}$$

So, the final value for velocity, pressure, and density of the ith particle will be, respectively, $\boldsymbol{V}_{fi} = \boldsymbol{V}_i + \Delta \boldsymbol{V}_i$, $p_{fi} = p_i + \Delta p_i$, and $\rho_{fi} = \rho_i + \Delta \rho_i$.

2.5 Boundary Conditions. Two types of boundary condition have been applied in the present study; dummy particles applied for wall boundaries and periodic boundary condition applied for flow boundaries. Dummy particles have widely been used to impose wall boundary condition [11,30,32,33]. For the present study, the dummy particles have been distributed similar to those applied by Lee et al. [11]; three layers of dummy particles with the same velocity of the wall particles (due to no slip condition) have been arranged nearby each wall boundary. Dummy particles scheme creates a condition very close to the no-slip boundary condition. Lee et al. [11] proposed a proper scheme for the dummy particles arrangement especially for the vertical corners. These particles have also the same pressure of the wall in the normal direction to satisfy the Neumann boundary condition. For the periodic boundary condition, each particle exited from the outlet is copied at the same position within the section at the inlet.

A pseudocode of the present solution algorithm is shown in Table 1. C, α, and ε are controlling parameters for the present algorithm. Selecting the proper value for each of them affects on the convergence rate and accuracy. C should be so big that the incompressibility is guaranteed. α is the time-step coefficient for calculation the intermediate time-step. Proper selection of α reduces the divergence errors. It is assumed that the pressure is constant during each time-step. So, the pressure at $t + \alpha \Delta t$ is equal to that at $t + \Delta t$. It is better that α is selected close to 1. However, when α equals to 1, the algorithm loses its flexibility. Our experience shows that $\alpha = 0.8$ can be a proper value to satisfy both of the convergence and accuracy. ε should be selected so big that the homogeneous particles distribution is provided. However, increasing ε increases the approximation in the flow field and reduces the accuracy. So, it is assumed that ε varies between 0 and 0.1;

Table 1 Algorithm of the present WCSPH method

```
for each time-step n do
  find the neighboring particles;
  apply the periodic boundary condition (if defined);
  for each particle i do
    compute V_i^{*,n+1} using Eq. (20);
    calculate ∀^{*,n+1} using Eq. (22);
    if i is an internal or wall particle then
      calculate pressure using Eq. (23);
    else (if i is a dummy particle)
      update pressure of dummy particles;
    end if
    correct velocity using Eq. (24);
    correct volume using Eq. (25);
    correct density using Eq. (26);
    update the position using Eq. (27);
    if i is an internal particle then
      shift the position by Δr_i evaluated from Eq. (29);
      correct the velocity, pressure, and density using Eqs. (31)–(33);
    end if
  end for
end for
```

$0 < \varepsilon \leq 0.1$. ε is selected according to the problem complexity; because of the major changes in the flow field due to rigid body motion, ε is selected between $0.08 \leq \varepsilon \leq 0.1$ for the present simulations.

For the present simulations, smoothing length is about three times of the initial particles space; $h = 3\delta$. Fatehi and Manzari [15] showed that first order discretization according to Eq. (4) satisfies convergence properly and second-order discretization according to Eq. (6) has conditional convergence; according to their investigation for Eq. (6), $2.5 < h/\delta < 3.5$ is proper if the particle space is adequately small.

3 Results and Discussion

To show the accuracy of the present algorithm to simulate different fluid flows, three different cases are examined; the first case is the simulation of the flow in the lid driven cavity for two Reynolds number values of 400 and 1000. The second case consists of a translating square cylinder in an initially stationary fluid in a rectangular cavity and the third case is the flow modeling of the transversely oscillating circular cylinder in the fully developed channel flow.

3.1 Lid Driven Cavity. The lid driven cavity is a well-known test for incompressible viscous fluid flow. The test case consists of the motion fluid inside a square cavity whose upper wall moves horizontally. The fluid is initially at rest and no-slip boundary condition is applied for all sides. Two different Reynolds numbers 400 and 1000, based on the lid velocity (U_w) and the size of the cavity side (L), are studied. Since the method is transient, the results are reported at $t^* = Ut/L = 60$. In this time, the variation of the flow field is almost vanished. So, it can be compared with the steady state results. In Fig. 1, the nondimensional horizontal (u_x/U_w) and vertical (u_y/U_w) velocity components are, respectively, plotted in the vertical and horizontal middle section of the cavity for different particles numbers in comparison with the data of Ghia et al. [34], ISPH results reported by Xu et al. [31] and standard WCSPH reported by Lee et al. [11]. Other solution parameters are $C/U_{\max} = 100$, $\alpha = 0.8$, and $\varepsilon = 0.08$.

For a quantitative comparison, the average deviation from the results of Ghia et al. [34] is defined as follows:

$$\mathrm{Err}(X) = \sqrt{\frac{1}{N}\sum_{i=1}^{N}\left(\frac{X_{\mathrm{ref}_i} - X_i}{X_{\mathrm{ref}_i}}\right)^2} \tag{34}$$

where X is the arbitrary variable, N is the number of points, and X_{ref} is the reference value reported by Ghia et al. [34]. For the case: $\mathrm{Re} = 1000$ with 160×160 particles, $\mathrm{Err}(u_x/U_w)$ and $\mathrm{Err}(u_y/U_w)$ calculated for the present results in comparison with ISPH results [31] and WCSPH results [11] are shown in Table 2. As shown here, the results have good agreement with the data of Ghia et al. [34] and are even better than those obtained by ISPH. As mentioned before, the main aim of the present method is to remove the nonphysical fluctuations of WCSPH. The accuracy is significantly improved and the fluctuations are removed in comparison with the standard WCSPH results reported by Lee et al. [11]. The fluctuations in the velocity profiles are clearly observed in the standard WCSPH especially in the case with 40×40 particles. However, the present method appropriately reduces these nonphysical fluctuations. It should be noted that Lee et al. [11] did not use particle shifting and kernel gradient correction for their simulations. This figure also shows the convergence process well; increasing the particles number increases the accuracy. The streamlines for two Reynolds numbers 400 and 1000 have also been shown in Fig. 2. It can be clearly seen that the simulations using the proposed method properly reveal all of the vortices, especially the vortices appeared in the corners of the cavity.

3.2 Moving Square Cylinder in an Initially Stationary Fluid. The second case considered consists of a translating square cylinder in a rectangular cavity. The results of Lee et al. [28] obtained from an incompressible finite difference method (FDM) are selected to validate the results. The coordinate system adopted is indicated in the sketch in Fig. 3.

The square is moved rightward for $t > 0$ in two stages; first is the cylinder motion starting from rest and accelerating to a final steady maximum velocity ($t < 1$), and second is constant velocity motion ($1 \leq t < 8$). The no-slip condition is applied for all the wall boundaries [28]. The test case is investigated for flow at Reynolds numbers 50 and 150, based on the length of the square side and maximum velocity of the square. Contour of velocity magnitude for the present simulation and the reference solution [28] for $\mathrm{Re} = 150$ and $t = 8$ s is plotted in Fig. 4.

To compare quantitatively, the pressure drag coefficient for $\mathrm{Re} = 50$ and 150 are plotted in Fig. 5 for the present study and mentioned benchmark data. The pressure drag coefficient has been calculated from the equation

$$C_{\mathrm{D}} = \frac{|F_x|}{\frac{1}{2}\rho U_{\max}^2 L b} \tag{35}$$

where ρ is the fluid density, $U_{\max}$ is the maximum velocity of the cylinder, L is the cylinder side, and b is the transversal length of the prismatic surface [28]. The drag force F_x is calculated by

$$F_x = \int_A p\boldsymbol{n}_x \cdot d\boldsymbol{A} \tag{36}$$

where p is the pressure acting on the cylinder, $\boldsymbol{n}_x$ is x-direction unit vector, and A is area vector. The results of another particle method (FVPM [35]) and the standard WCSPH are also shown in this figure.

The standard WCSPH is based on Eqs. (11)–(14). It is necessary to mention that the shifting algorithm which is defined in Sec. 2.4 is also applied for the standard WCSPH. The convergence is not obtained without shifting algorithm. The results of proposed algorithm have good agreement with the benchmark data. As shown here, the present method has better agreement with the benchmark data than the FVPM method and standard WCSPH; the fluctuations are significantly decreased in the results of the present method. In this study, the number of particles is 20,000 (to be the same with that of Ref. [35]) and the solution parameters are $C/U_{\max} = 25$, $\alpha = 0.8$, and $\varepsilon = 0.1$. The fluctuations in the drag coefficient come from the pressure waves returning from

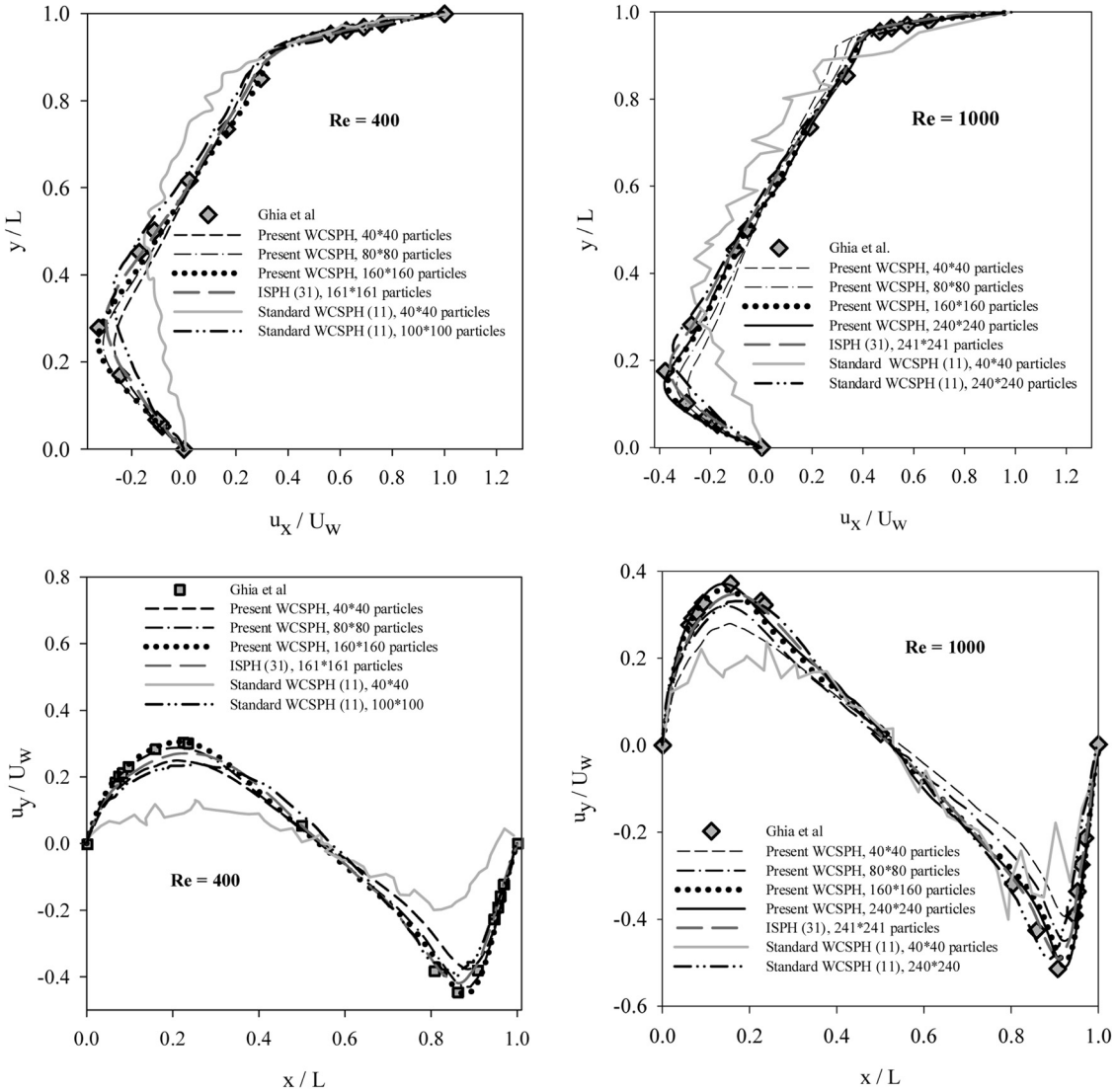

Fig. 1 The horizontal (above plots) and vertical (bottom plots) velocity profiles, respectively, in vertical and horizontal middle sections of the lid driven cavity for Re = 400 (left) and Re = 1000 (right)

the rectangular cavity walls. The present method somewhat overcomes these fluctuations in comparison with FVPM.

3.3 Flow Over the Stationary and Transversally Oscillating Cylinder. The last test case which is selected to examine the proposed algorithm is the numerical investigation of the flow behavior past a stationary and a transversely oscillating cylinder confined in a channel (Fig. 6). In the following, each of them is investigated separately. For all the cases, the particles number is about 90,000 and the ratio of the channel height to the cylinder diameter (H/D) and channel length to the cylinder diameter (L/D) are, respectively, 3 and 31.

Table 2 The root-mean-square of differences with results of Ghia et al. [34] for the case with 160 × 160 particles for the present results in comparison with ISPH results [31] and WCSPH results [11] for Re = 1000

	$\mathrm{Err}(u_x/U_w)$	$\mathrm{Err}(u_y/U_w)$
Present WCSPH	0.0899	0.0605
ISPH [31]	0.0822	0.1047
Standard WCSPH [11]	0.1925	0.1321

3.3.1 Stationary Case. In this case, the center of cylinder is fixed in 4D and 1.5D away from the inlet and the channel walls. No slip and periodic boundary conditions are, respectively, defined for wall and flow boundaries. To create fluid flow in a channel (without the cylinder), the body acceleration g_x can be imposed on the fluid particles. This acceleration generates a flow same as the case which $\Delta p = \rho g_x L$ applied on the ends of the

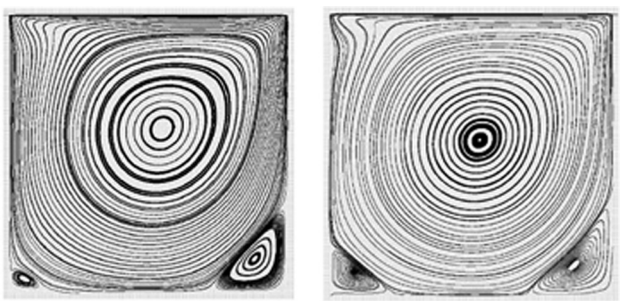

Fig. 2 The streamlines produced by the present SPH simulation for the cases with 160 × 160 particles for Re = 400 (left), Re = 1000 (right)

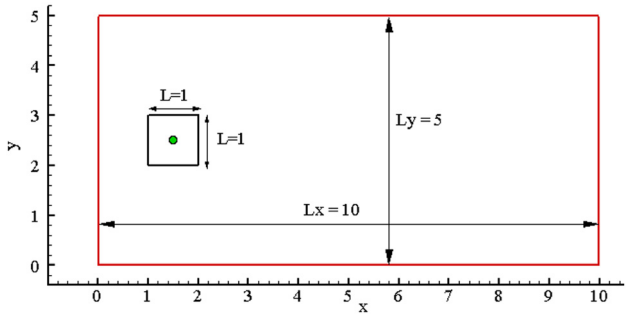

Fig. 3 Initial state ($t = 0$) of square in the rectangular cavity

channels. If the cylinder is added to the channel, according to superposition law, g_x will be

$$g_x = \frac{\Delta p_{\text{ch}} + \Delta p_{\text{cyl}}}{\rho L} = \frac{\Delta p_{\text{ch}} + \frac{1}{2} C_{\text{D}} \rho U_{\text{ave}}^2}{\rho L} \tag{37}$$

where Δp_{ch} is the pressure drop occurred in the channel and Δp_{cyl} is that due to the flow over the cylinder. Δp_{ch} can be approximated easily using U_{ave} (the average velocity magnitude in the inlet). So, to estimate g_x to achieve a desirable Reynolds number, it is necessary to estimate the C_{D} for that Reynolds number. However, this approximation might not certainly lead to the desirable Reynolds number. So, g_x is corrected via a linear proportional coefficient. The present periodic condition has also a difference with the standard form. The vortex stretching down the cylinder causes to deviate from the parabolic velocity profile at the outlet. So, a modified flow boundary condition is applied. The present flow boundary condition is similar with the periodic boundary condition. Except the velocity condition, the conditions which are necessary for the periodic boundary condition are imposed. However, velocity of the copied particles is modified according to the parabolic velocity profile. For each time-step, average velocity (U_{ave}) at the outlet section is calculated. Then, the velocity of the copied particle is modified as follows:

$$u_i = \frac{3}{2} U_{\text{ave}} \left(1 - \left(1 - \frac{2y_i}{H} \right)^2 \right) \tag{38}$$

A slightly modified periodic boundary condition has also been implemented by Shadloo et al. [36] for inlet and outlet particles in the direction of the flow.

Two Reynolds numbers 40 and 100 based on the cylinder diameter and average inlet velocity are considered for the stationary case and the results of the flow simulations according to the proposed algorithm are shown in Fig. 7. As expected, the vortices in the $\text{Re} = 40$ are symmetric and balanced and for $\text{Re} = 100$, the vortex shedding occurs.

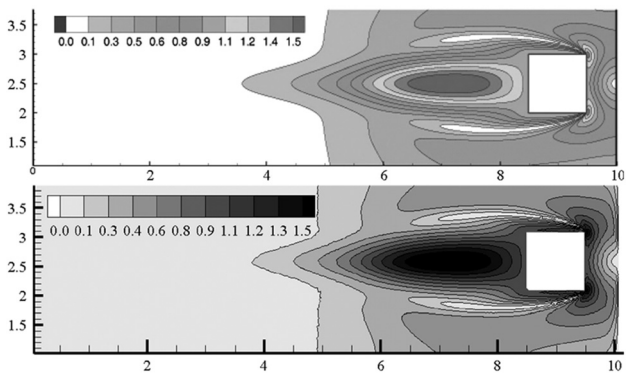

Fig. 4 Contour of the velocity magnitude of the force motion of the square for Re = 150 in the initially stationary flow for simulation of Lee et al. [28] (top) and present SPH algorithm simulation (bottom)

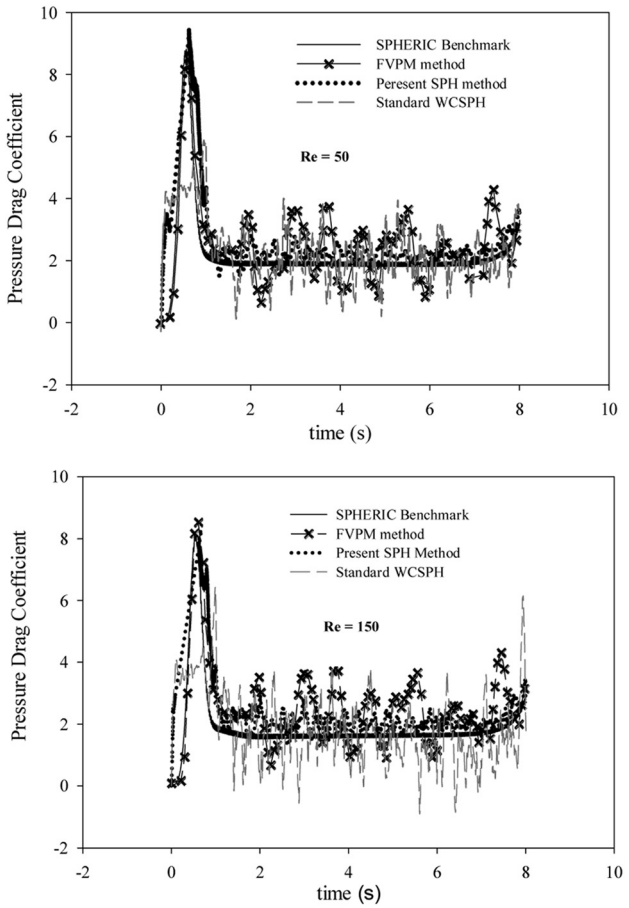

Fig. 5 Time variations of the pressure drag coefficient for incompressible FDM [28], FVPM [35], standard WCSPH, and present SPH method

The pattern of vorticity contour for the stationary case is plotted in Fig. 8. The vorticity is calculated by

$$\omega = \frac{\partial v}{\partial x} - \frac{\partial u}{\partial y} \tag{39}$$

where u and v are, respectively, horizontal and vertical components of the velocity.

In Fig. 9, the velocity profiles in the wake region for $\text{Re} = 40$ are compared with those reported by Ozalp and Dincer [37].

Recirculation length (L_{r}) and separation location are specified in Fig. 7. The dimensionless recirculation length (L_{r}/D) and

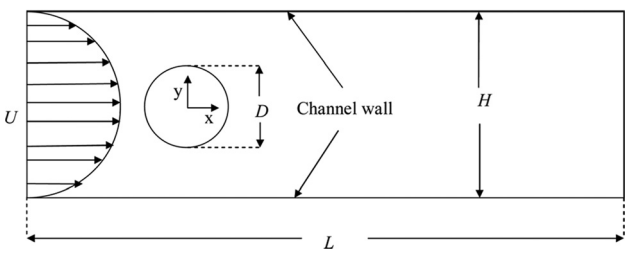

Fig. 6 Schematic of a channel confined flow over a circular cylinder

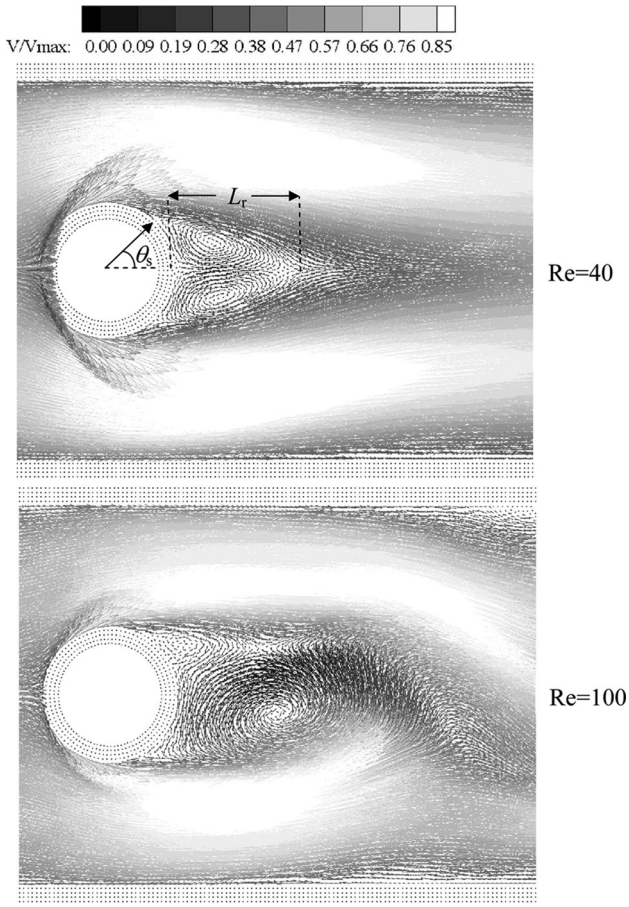

Fig. 7 SPH simulation of flow regimes past a stationary confined circular cylinder for Re = 40 and Re = 100

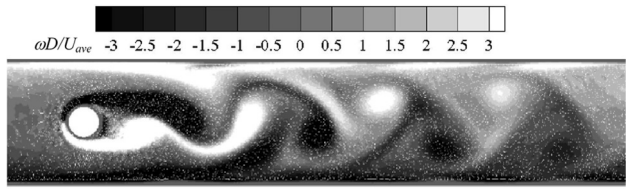

Fig. 8 Patterns of vorticity contour for stationary confined circular cylinder at Re = 100

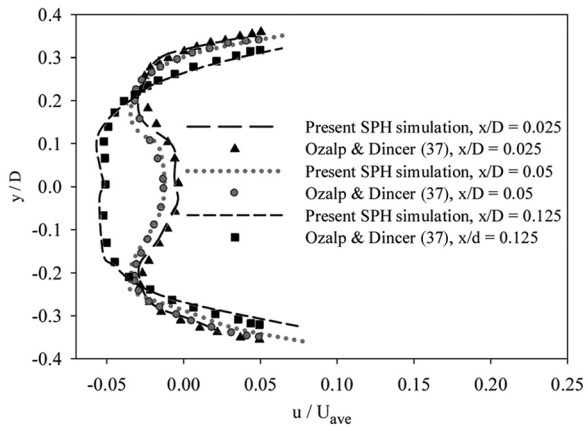

Fig. 9 Velocity profiles in the wake region for the Re = 40 case in comparison with the Ozalp and Dincer [37] data

Table 3 Comparison between present simulation and Ozalp and Dincer [37] results for dimensionless recirculation length and separation angle

	θ_s	L_r/D
Present study	49.41	1.111
Reference [37]	46	1.1825

Table 4 Comparison between the present simulation and data of Celik et al. [38] for Strouhal number and maximum lift force for the case Re = 100

	St	Maximum lift force
Present study	0.357	0.238
Reference [38]	0.36	0.247

separation location angle (θ_s) for the present simulation compared with those reported by Ozalp and Dincer [37] are shown in Table 3. The plot data have been nondimensionalized by the average velocity (U_{ave}) and cylinder diameter (D). For $Re = 100$, the Strouhal number ($St = f_0 D/U_{ave}$) and dimensionless lift force ($F_L/\rho U_{ave}^2 D$) for the present study and finite element results reported by Celik et al. [38] are compared in Table 4 (f_0 is the frequency of vortex shedding). The solution parameters are $C/U_{max} = 40$, $\alpha = 0.8$, and $\varepsilon = 0.08$.

3.3.2 Transversally Oscillating Cylinder. This case is similar with the stationary case, but the difference is that the cylinder oscillates in the y-direction. The analysis of the stationary case was necessary because the frequency of vortex shedding is required to adjust the motion of the cylinder in the transversely oscillating cylinder case; usually a dimensionless number like $F = f_f/f_0$ is defined to investigate the effect of the cylinder oscillation on the flow behavior (f_f is the frequency of the cylinder oscillation and f_0 is the vortex shedding frequency for the stationary cylinder case). Equation of cylinder oscillation is

$$y = y_{max} \sin(2\pi f_f t) \tag{40}$$

where $y_{max} = 0.4D$ is considered here as the oscillation amplitude.

In Table 5, the dimensionless lift forces for different F numbers are compared with those obtained by Celik et al. [38] using ALE method. As an example, the variation of dimensionless Lift force versus dimensionless time ($t^* = tU_{ave}/D$) for $F = 1.25$ is plotted in Fig. 10.

In Figs. 11 and 12, the contours of vorticity and streamlines for different F numbers in the case of $Re = 100$ are plotted. The effect of the F number on the vorticity pattern is clearly indicated in Fig. 11. Increasing the F number decreases the distance between two consecutive dark and light regions and increases the number of such regions. The von Karman streets created for different F numbers are shown in Fig. 12. The flow separation also causes to create some vortices near the channel walls.

Table 5 Maximum lift force in different *F* numbers for present study and results of Celik et al. [38]

Case	F	Maximum lift force
Present study	0.75	0.239
Reference [38]	0.75	0.24
Present study	1.0	0.96
Reference [38]	1.0	0.881
Present study	1.25	4.097
Reference [38]	1.25	4.03

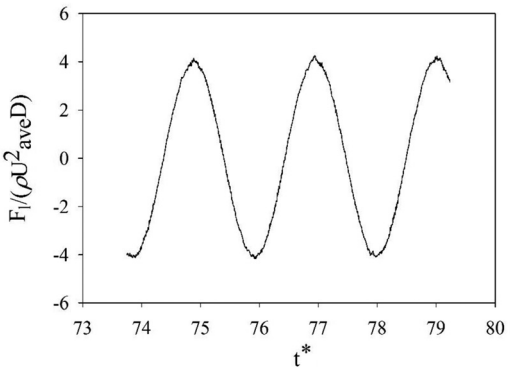

Fig. 10 Variation of nondimensional Lift force versus nondimensional time for $F = 1.25$

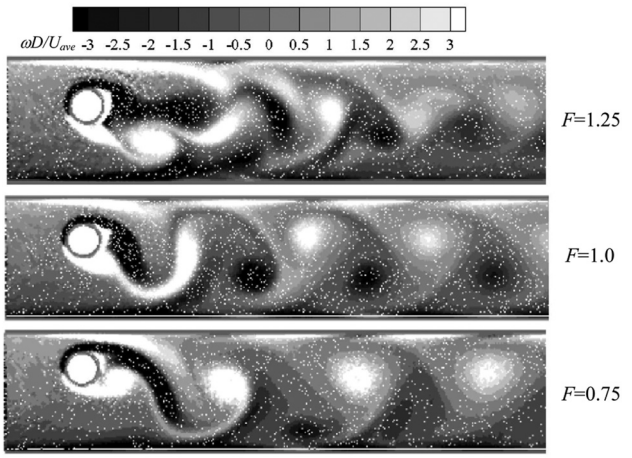

Fig. 11 Vorticity contours for flows with $F = 0.75$, $F = 1.00$, and $F = 1.25$ at Re = 100

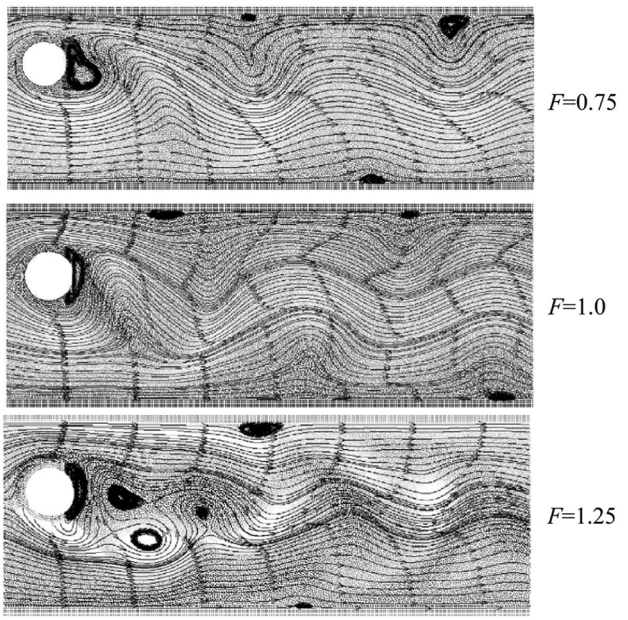

Fig. 12 Streamlines (von Karman streets) behind the oscillating cylinder for $F = 0.75$, $F = 1.00$, and $F = 1.25$ at Re = 100

4 Conclusion

In the present study, a robust modified weakly compressible smoothed particles hydrodynamic method based on a renormalized predictor–corrector scheme was introduced. The strong point of this algorithm is the combination of the most important modifications, such as velocity–pressure coupling for WCSPH, kernel gradient correction, and shifting algorithm. In order to achieve this, using the mass conservation equation, the divergence of the velocity is related to the Laplacian of the pressure. This correction helps to reduce the nonphysical pressure and density fluctuations and improves the accuracy. Because of this, the proposed algorithm can be used to model moving boundary problems and one way coupled FSIs. To show the ability of the proposed algorithm, three different cases were tested. In the first case, the lid driven cavity flow for two Reynolds numbers (400 and 1000) is considered. The effect of the number of particles on the convergence and accuracy is investigated. The results have good agreement with the benchmark data. The second case involved a moving square cylinder in the fluid which was initially at rest in a rectangular cavity. This case is rather a complex problem because the pressure waves which are returned from the rectangular walls usually cause the simulation to diverge. The present algorithm could remove this pressure waves; the results of pressure drag coefficient for two Reynolds numbers for the present study in comparison with another particle method (FVPM) and the standard WCSPH confirmed this claim. The last test case examined by the proposed algorithm was the numerical investigation of the flow behavior past a stationary and transversely oscillating cylinder confined in a channel; to study the effect of the cylinder oscillation on the flow, three different F numbers: $F = 0.75$, $F = 1.0$, and $F = 1.25$ are considered and the vorticity pattern and streamlines are compared.

Nomenclature

A = area vector
B = corrective tensor for kernel gradients
b = transversal length of the prismatic surface
C = speed of sound
C_D = drag coefficient
D = cylinder diameter
$\boldsymbol{e}_{ij}$ = the unit vector in the interparticle direction (from j to i)
Err = mean average error
f = arbitrary scalar function
f_f = frequency of the cylinder oscillation
f_0 = vortex shedding frequency
$\boldsymbol{F}$ = arbitrary tensor function
F = nondimensional frequency of cylinder motion
F_x = horizontal force
$\boldsymbol{g}$ = buoyancy acceleration
h = smoothing length
H = channel height
L = length
L_r = recirculation length
m = mass
n = time-step counter
$\boldsymbol{n}_x$ = x-direction unit vector
p = pressure
r = position vector
r' = subintegral variable
t = time
u = horizontal component of the velocity
v = vertical component of the velocity
$\boldsymbol{V}$ = velocity
W = weight or kernel function
X = arbitrary variable
$\forall_j$ = volume of jth particle
α, β_t = time-step coefficient
δ = initial particle space

δ_{min} = minimum distance between two neighboring particles
ε = displacement coefficient
θ_s = separation location angle
μ = viscosity
ν = kinematic viscosity
ρ = density

References

[1] Lucy, L. B., 1997, "A Numerical Approach to the Testing of the Fission Hypothesis," Astron. J., **82**, pp. 1013–1024.
[2] Gingold, R. A., and Monaghan, J. J., 1977, "Smoothed Particle Hydrodynamics: Theory and Application to Non-Spherical Stars," Mon. Not. R. Astron. Soc., **181**, pp. 375–389.
[3] Libersky, L., and Petschek, A. G., 1991, "Smooth Particle Hydrodynamics With Strength of Materials," Lect. Notes Phys., **395**, pp. 248–257.
[4] Monaghan, J. J., and Kocharyan, A., 1995, "SPH Simulation of Multi-Phase Flow," Comput. Phys. Commun., **87**(1), pp. 225–235.
[5] Muller, M., Schirm, S., and Teschner, M., 2004, "Interactive Blood Simulation for Virtual Surgery Based on Smoothed Particle Hydrodynamics," Technol. Health Care, **12**(1), pp. 25–31.
[6] Monaghan, J. J., 1994, "Simulating Free Surface Flows With SPH," J. Comput. Phys., **110**(2), pp. 399–406.
[7] Morris, J. P., 2000, "Simulating Surface Tension With Smoothed Particle Hydrodynamics," Int. J. Numer. Meth. Fluids, **33**(3), pp. 333–353.
[8] Cummins, S., and Rudman, M., 1999, "An SPH Projection Method," J. Comput. Phys., **152**(1), pp. 584–607.
[9] Shao, S. D., and Lo, E. Y. M., 2003, "Incompressible SPH Method for Simulating Newtonian and Non-Newtonian Flows With a Free Surface," Adv. Water Resour., **26**(7), pp. 787–800.
[10] Koshizuka, S., and Oka, Y., 1996, "Moving Particle Semi-Implicit Method for Fragmentation of Incompressible Fluid," Nucl. Sci. Eng., **123**(3), pp. 421–434.
[11] Lee, E. S., Moulinec, C., Xu, R., Laurence, D., and Stansby, P., 2008, "Comparisons of Weakly Compressible and Truly Incompressible Algorithms for the SPH Mesh Free Particle Method," J. Comput. Phys., **227**(18), pp. 8417–8436.
[12] Bonet, J., and Lok, T. S., 1999, "Variational and Momentum Preservation Aspects of Smooth Particle Hydrodynamic Formulation," Comput. Methods Appl. Mech. Eng., **180**(1–2), pp. 97–115.
[13] Rodriguez-Paz, M. X., and Bonet, J., 2004, "A Corrected Smooth Particle Hydrodynamics Method for the Simulation of Debris Flows," Numer. Methods Partial Differ. Equations, **20**(1), pp. 140–163.
[14] Shadloo, M. S., Zainali, A., Yildiz, M., and Suleman, A. R., 2012, "A Robust Weakly Compressible SPH Method and Its Comparison With an Incompressible SPH," Int. J. Numer. Methods Eng., **89**(8), pp. 939–956.
[15] Fatehi, R., and Manzari, M. T., 2011, "Error Estimation in Smoothed Particle Hydrodynamics and a New Scheme for Second Derivatives," Comput. Math. Appl., **61**(2), pp. 482–498.
[16] Fatehi, R., and Manzari, M. T., 2011, "A Remedy for Numerical Oscillations in Weakly Compressible Smoothed Particle Hydrodynamics," Int. J. Numer. Methods Fluids, **67**(9), pp. 1100–1114.
[17] Hu, X. Y., and Adams, N. A., 2007, "An Incompressible Multi-Phase SPH Method," J. Comput. Phys., **227**(1), pp. 264–278.
[18] Hu, X. Y., and Adams, N. A., 2009, "A Constant-Density Approach for Incompressible Multi-Phase SPH," J. Comput. Phys., **228**(6), pp. 2082–2091.
[19] Sadek, S. H., and Yildiz, M., 2013, "Modeling Die Swell of Second-Order Fluids Using Smoothed Particle Hydrodynamics," ASME J. Fluids Eng., **135**(5), p. 051103.
[20] Jiang, T., Ouyang, J., Zhang, L., and Jin-Lian, R., 2012, "The SPH Approach to the Process of Container Filling Based on Non-Linear Constitutive Models," Acta Mech. Sin., **28**(2), pp. 407–418.
[21] Kajtar, J. B., and Monaghan, J. J., 2012, "On the Swimming of Fish Like Bodies Near Free and Fixed Boundaries," Eur. J. Mech. B, **33**, pp. 1–13.
[22] Hashemi, M. R., Fatehi, R., and Manzari, M. T., 2012, "A Modified SPH Method for Simulating Motion of Rigid Bodies in Newtonian Fluid Flows," Int. J. Nonlinear Mech., **47**(6), pp. 626–638.
[23] Hashemi, M. R., Fatehi, R., and Manzari, M. T., 2011, "SPH Simulation of Interacting Solid Bodies Suspended in a Shear Flow of an Oldroyd-B Fluid," J. Non-Newton. Fluid, **166**(21–22), pp. 1239–1252.
[24] Cohen, R. C. Z., Cleary, P. W., and Mason, B. R., 2012, "Simulations of Dolphin Kick Swimming Using Smoothed Particle Hydrodynamics," Hum. Mov. Sci., **31**(3), pp. 604–619.
[25] Yang, J., and Stern, F., 2014, "A Sharp Interface Direct Forcing Immersed Boundary Approach for Fully Resolved Simulations of Particulate Flows," ASME J. Fluids Eng., **136**(4), p. 040904.
[26] Raman, S. K., Prakash, K. A., and Vengadesan, S., "Effect of Axis Ratio on Fluid Flow Around an Elliptic Cylinder—A Numerical Study," ASME J. Fluids Eng., **135**(11), p. 111201.
[27] Blom, F. J., and Leyland, P., 1998, "Analysis of Fluid–Structure Interaction by Means of Dynamic Unstructured Meshes," ASME J. Fluids Eng., **120**(4), pp. 792–798.
[28] Lee, E. S., Violeau, D., Laurence, D., Stansby, P., and Moulinec, C., 2007, "SPHERIC Test Case 6: 2-D Incompressible Flow Around a Moving Square Inside a Rectangular Box," SPHERIC 2nd International Workshop, Madrid, Spain, May 23–25, pp. 37–41.
[29] Capone, T., Panizzo, A., Cecioni, C., and Darlymple, A., 2007, "Accuracy and Stability of Numerical Schemes in SPH," 2nd SPHERIC International Workshop, A. J. C. Crespo, M. Gomez-Gesteira, A. Souto-Iglesias, L. Delorme, and J. M. Grassa, eds., Madrid, Spain, May 23–25, pp. 156–160.
[30] Morris, J. P., Fox, P. J., and Zhu, Y., 1997, "Modeling Low Reynolds Number Incompressible Flows Using SPH," J. Comput. Phys., **136**(1), pp. 214–226.
[31] Xu, R., Stansby, P., and Laurence, D., 2009, "Accuracy and Stability in Incompressible SPH (ISPH) Based on the Projection Method and a New Approach," J. Comput. Phys., **228**(18), pp. 6703–6725.
[32] Ma, J., Ge, W., Wang, X., Wang, J., and Li, J., 2006, "High-Resolution Simulation of Gas–Solid Suspension Using Macro-Scale Particle Methods," Chem. Eng. Sci., **61**(21), pp. 7096–7106.
[33] Xiong, Q., Li, B., Chen, F., Ma, J., Ge, W., and Li, J., 2010, "Direct Numerical Simulation of Sub-Grid Structures in Gas–Solid Flow-GPU Implementation of Macro-Scale Pseudo-Particle Modeling," Chem. Eng. Sci., **65**(19), pp. 5356–5365.
[34] Ghia, U., Ghia, K. N., and Shin, C. T., 1982, "High-Resolutions for Incompressible Flow Using the Navier–Stokes Equations and a Multigrid Method," J. Comput. Phys., **48**(3), pp. 387–411.
[35] Nestor, R., Basa, M., and Quinlan, N., 2008, "Moving Boundary Problems in the Finite Volume Particle Method," 3rd ERCOFTAC SPHERIC Workshop on SPH Applications, Lausanne, Switzerland, June 4–6, pp. 109–114.
[36] Shadloo, M. S., Zainali, A., Sadek, S. H., and Yildiz, M., 2011, "Improved Incompressible Smoothed Particle Hydrodynamics Method for Simulating Flow Around Bluff Bodies," Comput. Methods Appl. Mech. Eng., **200**(9–12), pp. 1008–1020.
[37] Ozalp, A. A., and Dincer, I., 2010, "Laminar Boundary Layer Development Around a Circular Cylinder: Fluid Flow and Heat-Mass Transfer Characteristics," ASME J. Heat. Transfer, **132**(12), p. 121703.
[38] Celik, B., Raisee, M., and Beskok, A., 2010, "Heat Transfer Enhancement in a Slot Channel Via a Transversely Oscillating Adiabatic Circular Cylinder," Int. J. Heat Mass Transfer, **53**(4), pp. 626–634.